IMAGING TWO-PROTON CORRELATIONS IN THE PRESENCE OF LONG TIME SCALE EMISSION MECHANISMS

G. Verde, D.A. Brown[a], P. Danielewicz, C.K. Gelbke, W.G. Lynch, M.B. Tsang

During an energetic nucleus-nucleus collision, the emission of particles commences at the initial overlap of the projectile and target nuclei and continues as energy and momentum are progressively shared among interacting nucleons. Intensity interferometry is a unique and sensitive tool for investigating the early stages of such collisions when the dynamics are evolving rapidly [1,2]. At incident energies below the pion threshold, two-proton interferometry, pioneered by Koonin [3], provides the principal interferometric tool. The coupling of two-proton interferometry to various dynamical and statistical models of reaction mechanisms [4,5] has increased its predictive power and has illuminated many qualitative and quantitative features of two proton correlations and of heavy ion reactions [1,2].

Due to the attractive nature of the S-wave phase shift, the correlation function for two protons displays a maximum at a relative momentum of about 20 MeV/c that is the dominant feature of correlation functions for short lived and compact emitting regions (sources). It is often regarded as one of the most sensitive measures of the source size or lifetime because this maximum value is inversely proportional to the volume for a compact, zero lifetime source [1,2]. However, we show below that this maximum does not accurately reflect the size of the emitting source; instead, the maximum value reflects more directly the relative contributions from prompt and long time scale emission.The source size is more directly measured by the width of the peak. Using new imaging techniques [6,7] that allow the shape of the source to vary freely, we demonstrate these sensitivities by decomposing experimental two proton correlations for ^{14}N + ^{197}Au collisions at 75 MeV/u.

We begin by considering the angle-averaged correlation function, $C(q)$, for two protons with individual momenta $\vec{p}_1$ and $\vec{p}_2$ and relative momentum $q = |\vec{p}_1 - \vec{p}_2|/2$. Experimentally, the two proton correlation function $C(q)$ can be defined in terms of the coincidence yield $Y(\vec{p}_1, \vec{p}_2)$ and the single proton yields $Y(\vec{p}_1)$ and $Y(\vec{p}_2)$ [1,2]:

$$\Sigma Y(\vec{p}_1, \vec{p}_2) = k \cdot C(q) \cdot \Sigma \left[Y(\vec{p}_1) \cdot Y(\vec{p}_2) \right], \tag{1}$$

where the sum runs over values of $\vec{p}_1$ and $\vec{p}_2$ consistent with the relative momentum q. In this angle averaged sum, all angles between the relative momentum $\overrightarrow{q} = (\vec{p}_1 - \vec{p}_2)/2$ and the total momentum $\overrightarrow{p_{tot}} = \vec{p}_1 + \vec{p}_2$ are considered. The normalization constant k is determined by requiring $C(q) = 1$ at large q where final state interactions can be neglected. Theoretically, the angle averaged Koonin-Pratt equation [3-5]:

$$C(q) = 1 + R(q) = 1 + 4\pi \int dr r^2 K(q, r) S(r), \tag{2}$$

allows the calculation of this correlation function, $C(q)$, from the source function, $S(r)$, defined as the probability distribution for emitting a pair of protons. The variable r corresponds to the spatial separation between the two proton at the time the second proton is emitted [1,2]. The angle-averaged kernel $K(q, r)$, is calculated from the radial part of two-proton relative wave function and contains the information about how the two proton cross section is influenced by anti-symmetrization and by the two-proton nuclear and Coulomb final state interactions. As these factors are sensitive to the separation r, they provide a mechanism by which the source function $S(r)$ can be explored.

While Eq. (2) permits any form of source function, most analyses have assumed a Gaussian profile for $S(r)$, normalized to unity over all space and completely defined by a single parameter r_0 as follows:

$$S(r) = S_1(r, r_0) \equiv \frac{1}{(2\pi)^{3/2} r_0^3} \exp(-\frac{r^2}{2r_0^2}) \tag{3}$$

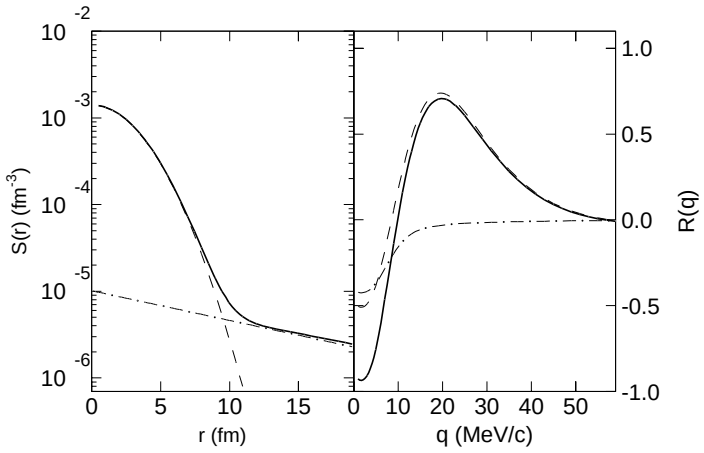

Figure 1: Left panel: The solid line indicates a typical two-proton source function for intermediate energy collisions. The dashed and dot-dashed lines provide a decomposition of the solid line into short and long time scale emissions respectively. Right panel: The solid, dashed and dot-dashed curves show the correlation functions corresponding to the source functions in the left panel.

where $\sqrt{3/2}r_0$ is the rms Gaussian source radius. For such Gaussian sources, r_0 and the peak value of the correlation function at 20 MeV/c are uniquely related. However, the assumption that this relationship is true, generally or even qualitatively, fails when one has both short and long time scale emissions.

The solid line on the left part of Fig. 1 shows a typical source function for intermediate energy heavy ion reactions. It generates a total two-proton correlation function corresponding to the solid line in the right panel of the figure. The total source has a short-ranged contribution approximated by the dashed line in the left panel, which is peaked at $r = 0$ and originates from fast pre-equilibrium emissions that dominate the earlier stages of the reaction. At such small distances, nuclear interactions make the dominant contribution to $K(q, r)$; the contribution to the total correlation function from this short-ranged contribution (dashed line, right panel) not surpisingly displays a large maximum at $q = 20MeV/c$.

In addition to these pre-equilibrium contributions, there is a long exponential tail at large r-values (dot-dashed line, left panel) that corresponds to the emission of one or both protons via long time scale secondary decays of excited nuclei like the heavy residues, which are produced in the same collision. The distance scale for such long time scale decays is given approximately by the mean velocity of evaporated protons times their mean emission lifetime. At such large distances, the Coulomb interaction and the Pauli principle are the dominant factors governing $K(q, r)$; the corresponding contribution to the total correlation (dot-dashed line, right panel) vanishes everywhere except the lowest relative momenta $q < 10MeV/c$. Two proton correlations at $q < 10MeV/c$ are rarely measured [8] with high precision, however, as they represent an extremely small and difficult-to-measure fraction of the total two-proton cross section.

As a practical matter, the similarity of the dashed and solid lines at $q < 10MeV/c$ in Fig. 1 makes it clear that one images primarily the preequilibrium portion of the source in such collisions. We have calculated correlation functions assuming that a fraction λ of the two proton source is pre-equilibrium in nature and Gaussian distributed, i.e. $S(r) = S_\lambda(r, r_0) = \lambda S_1(r, r_0)$. Even though $R(q)$ for $q > 10MeV/c$ depends almost entirely on the short-ranged pre-equilibrium contribution, the fact that $R(q)$ depends linearly on λ via the the source function $S_\lambda(r, r_0)$ introduces a sensitivity to the relative contributions from long time scale emission. The left panel of Fig. 2 shows three correlation functions generated by Gaussian sources with r_0 values of 2.0, 2.5 and 3.0 fm and different normalizations of $\lambda = 0.38, 0.61$ and 1, respectively, corresponding to different total pre-equilibrium contributions to the two proton source function. These three sets of source parameters provide yield identical peak values for the correlation function $C(q) = 1 + R(q)$ but have different source radii. This

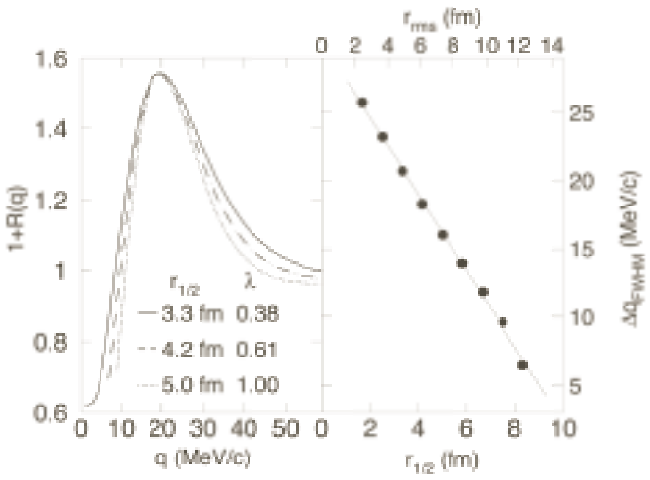

Figure 2: Left: The curves show correlation functions for Gaussian sources with various normalizations and radii, but with the same maximum value as discussed in the text. Right: The relationship between the with of the resonance peak at 20 MeV/c and the rms and half radii discused in the text. The line represents a best-fit interpolation of the calculated points.

demonstrates that the maximum value of the correlation alone is insufficient to disentangle its dual sensitivity to source radius r_0 and pre-equilibrium fraction λ.

The width of the correlation functions differ, however, with smaller sources generating correlation functions with wider peaks. This sensitivity is quantitatively demonstrated in the right panel in Fig. 2, which shows the correlation between Δq_{FWHM} (the full width at half maximum) and $R_{1/2}$, the radius where the source decreases to 1/2 of its maximum value. (For Gaussian sources, $R_{1/2} \approx 1.18 r_0$.) Indeed, Δq_{FWHM} is insensitive to λ by construction and accurately constrains the pre-equilibrium source radius. The additional information provided by the peak value of $C(q)$ can constrain the pre-equilibrium fraction λ, or alternatively, the source strength as $r \to 0$, $S(0)$ as suggested by Ref. [7].

To demonstrate that the conclusions drawn from of Fig. 2 are not artifacts of the Gaussian parameterization, we go beyond the limations of a two parameter (λ, r_0) analysis by numerically inverting experimental correlation functions as described by Refs. [6,7,11]. The data points in the left and right panels of Fig. 3 show proton-proton correlation functions measured by Gong et al. [9]. These data were measured at polar angles centered about $\theta_{cm} \simeq 25^0$ in ^{14}N+^{197}Au collisions at 75 MeV/u for three gates on the total laboratory momentum of the two protons centered at $P_{sum,c} = |\vec{p}_1 + \vec{p}_2|_{center} = 330,\ 615$ and 1035 MeV/c [10]. (Details of the experiment can be found in Ref. [9]).

The colored, dashed lines in the left panel of Fig. 3 correspond to the correlation functions calculated using Gaussian sources of the form $S_1(r, r_0)$ (no long time scale emission) and Eq. 2 following Ref. [9]. Consistent with the latter analyses, a strong momentum dependence in the values for r_0 of 5.9, 4.2 and 3.4 fm ($R_{1/2}$ of about 7.0, 5.0 and 4.0 fm) is required to reproduce the magnitude of the correlation at 20 MeV/c for protons with $P_{sum,c} = 330,\ 615$ and 1035 MeV/c, respectively [9]. The corresponding source functions are shown in Fig. 4 by the colored dashed lines. However, such Gaussian sources fail to reproduce the widths of the resonance peaks, especially for the lower total momenta, $P_{sum,c} = 330$ and 615, which is problematic because the widths probe directly the source radius.

The model dependence of such analyses were avoided by parameterizing the sources for these two proton correlations, for $0 \leq r \leq 20$ fm, by six 3^{rd}-order b-spline polynomials, following Ref. [11]. The numerical inversion of Eq. 2 was then achieved via the optimization algorithm of Ref. [7,11]. The thick color curves on the right panel of Fig. 3 show the best-fits of the experimental data with the imaging approach. The corresponding imaged sources are represented in Fig. 4 by bands of the same color. The widths of these curves represent the

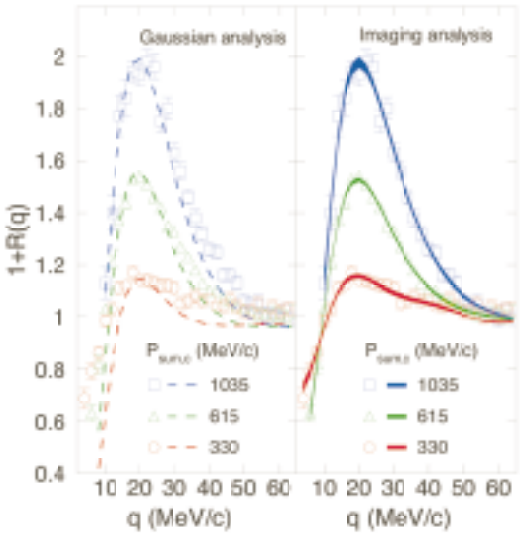

Figure 3: The data points refer to the experimental correlation functions measured in ^{14}N+^{197}Au reactions at E/A=75 MeV. The colored dashed lines and the colored bands correspond to the fit produced with the Gaussian analysis (left panel) and the imaging analysis (right panel), respectively, as discussed in the text.

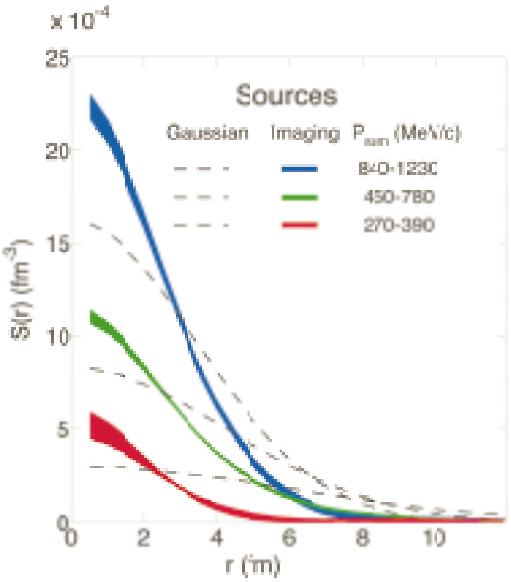

Figure 4: The red, green and blue dashed lines indicate source functions corresponding to the Gaussian fits at the momentum gates shown in the left panel of Fig. 3. The red, green and blue shaded areas indicate the source functions corresponding to the fits on the right panel Fig. 3 that were obtained by the numerical inversion discussed in the text.

lower and upper limits defined by the one sigma error bars of the extracted source functions.

The imaging technique reproduces both the strong momentum dependence of the magnitude and the weak momentum dependence of the width of the peak at 20 MeV/c. Consistent with the weak momentum dependence of the widths, the extracted source radius varies little with $P_{sum,c}$; values for $R_{1/2}$ of 2.4, 3.1 and 2.9 fm are obtained for $P_{sum,c} = 330,\ 615$ and 1035 MeV/c, respectively, and are much smaller than the half radii $R_{1/2}$ of 7.0, 5.0 and 4.0 fm, respectively, determined by the corresponding Gaussian source analysis in the limit $\lambda = 1$. Indeed, direct examinations of the three correlation functions yields widths of about $\Delta q_{FWHM} \approx$ 20 MeV/c corresponding to source radii of about $R_{1/2}\approx$2.7 fm ($r_0 \approx 2.3$ fm) when the systematics of Fig. 2 are invoked. That the values for $R_{1/2}$ extracted from Δq_{FWHM} and Fig. 2 differ from those of the multi-parameter imaging technique reflects the fact that the imaged sources do not have Gaussian profiles like the ones employed to construct Fig. 2.

Even though long lifetime emission mechanisms mainly influence the shape of $R(q)$ at small and usually unmeasured relative momenta, the extracted normalization λ provides stringent constraints on the pre-equilibrium fraction of the proton yield, f_{pre}. Since λ represents the total probability that both protons are of pre-quilibrium origin, the extracted values for $\lambda = 0.09, 0.45$ and 0.6 for $P_{sum,c} = 330,\ 615$ and 1035 imply corresponding values for $f_{pre} = \sqrt{\lambda} = 0.3, 0.68$ and 0.78 for the fractions of the single proton yield that are preequilibrium and complimentary values $1 - \sqrt{\lambda} = 0.7, 0.32$ and 0.22 for the fractions that are not. The availability of such information from correlation function analyses is unique and of extraordinary utility to the application of correlation function analyses to the testing of transport theoretical descriptions of nucleus-nucleus collisions [12]. It is also of prime importance to the interpretion of multifragmentation and other fragment production mechanisms where the role of secondary decay is not understood well enough to allow quantitative comparisons with theoretical models [13].

In summary, we have examined the role that long time scale decays play in two proton correlation functions. We find that when both rapid pre-equilibrium emission and long time scale evaporative emission are present, most correlation functions permit only the imaging of the pre-equilibrium source. The presence of long time scale emission destroys the correlation between source size and the maximum at 20 MeV/c; source size information is primarily preserved in the width of the correlation maximum. Further analysis provide important information about the relative importance of pre-equilibirum and long time scale emission. We confirm these ideas via a detailed multi-parameter analysis of experimental correlation functions that allows one to avoid the limitation and model dependences of Gaussian sources. Such analyses promise significant improvements in the description of correlation functions and their uses to quantitative probe nuclear reactions.

This work was supported by the National Science Foundation under Grant Nos. PHY-95-28844 and PHY-0070818.

a: Lawrence, Livermore National Laboratory, Livermore, CA 94551-0808 USA.

References

1. D.H. Boal, C.-K. Gelbke and B.K. Jennings, Rev. Mod. Phys. 62, 553 (1990).
2. W. Bauer, C.K. Gelbke, and S. Pratt, Ann. Rev. Nucl. Part. Sci, 42, 77 (1992).
3. S.E. Koonin, Phys. Lett. B**70**, 43 (1977).
4. S. Pratt and M.B. Tsang, Phys. Rev. C**36**, 2390 (1987).
5. W.G. Gong *et al.*, Phys. Rev. C**43**, 781 (1991).
6. D.A. Brown and P. Danielewicz, Phys. Lett. B**398**, 252 (1997).
7. D.A. Brown and P. Danielewicz, Phys. Rev. C**57**, 2474 (1998).
8. L. Martin *et al.*, Nucl. Phys. A 583, C407 (1995).
9. W.G. Gong *et al.*, Phys. Rev. C**43**, 1804 (1991), and ref. therein.
10. The momentum gates corresponding to $P_{sum,c} = 330, 615$ and 1035 are $P_{sum} =$ 270-390, 450-780 and 840-1230.
11. D.A. Brown and P. Danielewicz, nucl-th/0010108 (2000).
12. D.O. Handzy *et al.*, Phys. Rev. Lett. 75, 2916 (1995).
13. S. R. Souza *et al.*, Phys. Rev. C 62, 064607 (2000).